Shape and energy spectra of Λ hypernuclei from a Skyrme-Hartree-Fock model and a beyond-mean-field calculation

Ji-Wei Cui,[1] Xian-Rong Zhou,[1,2,*] and Hans-Josef Schulze[3]

[1]*Department of Physics and Institute of Theoretical Physics and Astrophysics, Xiamen University, Xiamen 361005, People's Republic of China*

[2]*State Key Laboratory of Theoretical Physics, Institute of Theoretical Physics, Chinese Academy of Sciences, Beijing 100190, China*

[3]*Sezione INFN, Dipartimento di Fisica, Universitá di Catania, Via Santa Sofia 64, I-95123 Catania, Italy*

(Received 16 February 2015; revised manuscript received 24 March 2015; published 8 May 2015)

A triaxial shape-constrained Skyrme-Hartree-Fock mean-field model, employing a density-dependent pairing interaction and the NSC89 $N\Lambda$ interaction, is used to investigate the potential energy surfaces of the Λ hypernuclei ${}^{13}_{\Lambda}$C, ${}^{21}_{\Lambda}$Ne, ${}^{25,27}_{\Lambda}$Mg, and ${}^{27,29}_{\Lambda}$Si. Angular momentum projection and particle number projection techniques are applied to the axially deformed mean-field states to restore the symmetries lost in the mean-field calculation, and the energy spectra and $E2$ transition probabilities of several (hyper)nuclei are studied, demonstrating the shrinkage effect of the Λ, which is analyzed in detail.

DOI: 10.1103/PhysRevC.91.054306 PACS number(s): 21.80.+a, 21.60.Jz, 23.20.Lv

I. INTRODUCTION

The investigation of Λ hypernuclei has achieved great progress since their first discovery [1]. One of the topics in this research field is how the addition of a Λ hyperon, as an impurity, affects the nuclear system, since the Λ hyperon can be deeply bound in atomic nuclei because of the absence of Pauli blocking. In the laboratory, several kinds of phenomena have been observed once a Λ is added: The Λ can introduce spin splitting in the atomic nucleus, which is observed in ${}^{13}_{\Lambda}$C [2], while a shrinkage due to the glue-like effect of the Λ is observed for ${}^{7}_{\Lambda}$Li [3].

Meanwhile, the theoretical study of Λ hypernuclei has made important progress and various models have been developed to describe the properties of such systems. For light Λ hypernuclei, besides the shell-model calculations [4–7], which interpret the results of γ-ray experiments [8], the N-body cluster model [9] and the antisymmetrized molecular dynamics (AMD) method [10] reproduce the energy spectra and transition probabilities very well. The N-body cluster model divides a Λ hypernucleus into several nuclear clusters and a Λ, and is very successful for the study of p-shell hypernuclei [9,11,12] and even double-Λ hypernuclei [13]. However, the problem of dimensionality of Jacobi coordinates makes it difficult for this model to describe Λ hypernuclei beyond the p shell. For sd-shell nuclei, the AMD method, which combines intrinsic wave functions with angular momentum projection (AMP) techniques and the generator coordinate method (GCM), gives comprehensive energy spectra with both positive and negative parities, especially for ${}^{21}_{\Lambda}$Ne [14] and ${}^{25}_{\Lambda}$Mg [15,16].

Nonrelativistic and relativistic mean-field (RMF) models [17] can also describe a Λ hypernuclear system very well, in particular for very heavy systems. There are several examples in which multidimensionally constrained RMF models investigate shape evolution of some Λ hypernuclei [18] and clusterization in superdeformed hypernuclei [19]. Recently, hyperonic RMF models were also extended to investigate the low-lying states of hypernuclei based on the particle-rotor model [20] and the impurity effect based on the five-dimensional collective Hamiltonian (5DCH) model [21].

The Skyrme-Hartree-Fock (SHF) model, which is the focus of this paper, has been extensively used to study Λ hypernuclei in a vast mass region, using various kinds of density-dependent $N\Lambda$ interactions [22–28]. In these studies, microscopic $N\Lambda$ potentials in the form of density functionals, and derived from Brueckner-Hartree-Fock (BHF) calculations of isospin-asymmetric hypernuclear matter with the Nijmegen soft-core hyperon-nucleon potentials [29,30], were used. In the framework of a spherical SHF model, hyperonic binding energies of various Λ and double-Λ hypernuclei were obtained and compared with experimental values [27,28]. Recently, the shape-constrained SHF model with pairing force was introduced to investigate axially deformed Λ hypernuclei and drip line properties [24–26].

Another kind of density-dependent $N\Lambda$ potential is a Skyrme-type $N\Lambda$ interaction given in complete analogy with the nuclear Skyrme interaction [31]. This kind of interaction was used to investigate the shape of Λ hypernuclei in the full (β,γ) deformation with a shape-constrained SHF+BCS method [32]. Such an energy density functional (EDF) model was also extended to the 5DCH model [33], which is the first realization of the idea to study the hyperon impurity effect on nuclear collective excitations at the beyond-mean-field (BMF) level with EDF methods. One motivation of the current article is extending the SHF+BCS calculation employing density-dependent Nijmegen soft-core hyperon-nucleon potentials to triaxial deformation, in order to study the changes of potential energy surfaces (PES) in the (β,γ) plane due to the addition of a Λ.

Although the hypernuclear mean-field models, including the RMF model and SHF+BCS model, give very reasonable descriptions of hypernuclear properties, angular momentum conservation in the intrinsic-frame calculation is broken, and furthermore the BCS approximation does not conserve particle number [34]. Such drawbacks make the hypernuclear mean-field models unable to describe the energy spectrum or

*Corresponding author: xrzhou@xmu.edu.cn

the transition probabilities, which are both observables in the laboratory-fixed reference frame. To this end, the AMP and particle number projection (PNP) techniques [35] are needed to restore the symmetries lost in the mean-field calculation, and that is another motivation of this article. It is the first time employing a projected SHF+BCS model to calculate the single-Λ hyperonic spectra and $E2$ transition probabilities, and it is a complement of the recent step made in the same direction on the basis of a relativistic EDF [20].

In this work we focus on the hypernuclei ${}^{13}_{\Lambda}$C [2,11,14,17, 18,24,26,32], ${}^{21}_{\Lambda}$Ne [14], ${}^{25,27}_{\Lambda}$Mg [15,16,18,21,32,33], and ${}^{27,29}_{\Lambda}$Si [17,18,32], which where also studied in different approaches and are thus of major interest for comparison.

This paper is organized as follows. In Sec. II, the hypernuclear SHF+BCS mean-field approach and the AMP and PNP techniques are introduced. Sec. III presents the results and discussion for p- and sd-shell hypernuclei. In Sec. IV, we give the conclusions and an outlook.

II. FORMALISM

There are mainly two parts in our approach. The first is the mean-field calculation based on the self-consistent deformed SHF method solved in harmonic-oscillator basis [36], using the NSC89 $N\Lambda$ interaction [28]. The second one is the angular-momentum and particle-number restoration of mean-field states using the AMP and PNP techniques.

The total energy of a hypernucleus in the SHF model is expressed as

$$E = \int d^3r\,(\varepsilon_N + \varepsilon_\Lambda), \tag{1}$$

where ε_N is the energy functional of the core nucleus and ε_Λ is the gain of energy density due to the addition of one Λ. ε_N is the standard Hamiltonian density of the Skyrme interaction [37] and ε_Λ is divided into two parts [28],

$$\varepsilon_\Lambda = \frac{\tau_\Lambda}{2m^*_\Lambda(\rho_N,\rho_\Lambda)} + \varepsilon^*_{N\Lambda}(\rho_N,\rho_\Lambda), \tag{2}$$

where the first term represents the kinetic energy of the Λ and the second term is

$$\varepsilon^*_{N\Lambda}(\rho_N,\rho_\Lambda) = \varepsilon_{N\Lambda}(\rho_N,\rho_\Lambda) - \left(\frac{m_\Lambda}{m^*_\Lambda(\rho_N,\rho_\Lambda)} - 1\right)\frac{C\rho_\Lambda^{5/3}}{2m_\Lambda}, \tag{3}$$

where $\varepsilon_{N\Lambda}(\rho_N,\rho_\Lambda)$ is the $N\Lambda$ bulk energy density extracted from BHF calculations of homogeneous hypernuclear matter and the constant $C = (3/5)(3\pi^2)^{2/3} \approx 5.742$ has been introduced [28]. Through the variation of the total energy in Eq. (1), one derives the SHF Schrödinger equation for both nucleons and Λ,

$$\left[\nabla\cdot\frac{1}{2m^*_\tau(\boldsymbol{r})}\nabla - V_\tau(\boldsymbol{r}) + i\boldsymbol{W}_\tau(\boldsymbol{r})\cdot(\nabla\times\boldsymbol{\sigma})\right]\phi^i_\tau(\boldsymbol{r}) = e^i_\tau\phi^i_\tau(\boldsymbol{r}), \tag{4}$$

with the mean fields

$$V_N = V_N^{\mathrm{SHF}} + \frac{\partial\varepsilon^*_{N\Lambda}}{\partial\rho_N}, \tag{5}$$

$$V_\Lambda = \frac{\partial\varepsilon^*_{N\Lambda}}{\partial\rho_\Lambda}. \tag{6}$$

V_N^{SHF} is the Skyrme mean field for nucleons and $\boldsymbol{W}_N$ is the nucleonic spin-orbit mean field. V_Λ is the Λ hyperonic mean field and the hyperonic spin-orbit term $\boldsymbol{W}_\Lambda$ is excluded from the mean-field calculation due to its small spin-orbit splitting justified by experimental observations [2,38,39]. The two important quantities in the $N\Lambda$ interaction, $\varepsilon_{N\Lambda}$ and m^*_Λ, are expressed respectively as

$$\begin{aligned}\varepsilon_{N\Lambda} \approx &-\left(\varepsilon_1 - \varepsilon_2\rho_N + \varepsilon_3\rho_N^2\right)\rho_N\rho_\Lambda \\ &+ \left(\varepsilon_4 - \varepsilon_5\rho_N + \varepsilon_6\rho_N^2\right)\rho_N\rho_\Lambda^{5/3} \\ &- \left(\varepsilon_7 - \varepsilon_8\rho_N + \varepsilon_9\rho_N^2\right)\rho_\Lambda^2,\end{aligned} \tag{7}$$

$$\frac{m^*_\Lambda}{m_\Lambda}(\rho_N) \approx \mu_1 - \mu_2\rho_N + \mu_3\rho_N^2 - \mu_4\rho_N^3. \tag{8}$$

The parameters ε_i and μ_i are taken from Ref. [28] for different $N\Lambda$ potentials.

Beyond the nucleonic mean-field, the BCS approximation is used, employing a density-dependent pairing force with the pairing strength [40,41]

$$G(\boldsymbol{r}) = V_0\left[1 - \frac{\rho(\boldsymbol{r})}{\rho_0}\right]. \tag{9}$$

Pairing takes part in the self-consistent calculation via multiplying the densities ρ, τ, $\boldsymbol{J}$ by the occupation probabilities v_i^2.

The mean-field calculation above gives single-particle energies, e^i_τ, and ground states in the intrinsic frame. The intrinsic ground state is written as

$$|\psi\rangle = |\varphi\rangle_N \otimes |\varphi\rangle_\Lambda \tag{10}$$

with $|\varphi\rangle_N$ and $|\varphi\rangle_\Lambda$ being wave functions of the nuclear core and the hyperon, respectively. Then the AMP and PNP operators are applied to obtain a symmetry-conserving wave function

$$|IMK\rangle = \hat{P}^I_{MK}\hat{P}^n\hat{P}^z|\psi\rangle. \tag{11}$$

The AMP operators $\hat{P}^I_{MK}$ are composed of Wigner functions $D^I_{MK}(\Omega)$ and the space-rotational operator $\hat{R}(\Omega)$ as in Ref. [42],

$$\hat{P}^I_{MK} = \frac{2I+1}{8\pi^2}\int d\Omega\, D^I_{MK}\hat{R}(\Omega), \tag{12}$$

where Ω represents the three Euler angles (α,β,γ). The PNP operators for neutrons and protons have a similar form [35],

$$\hat{P}^q = \frac{1}{2\pi}\int d\varphi\, e^{i\varphi(\hat{q}-q_0)}, \tag{13}$$

where φ is the gauge angle.

The intrinsic quantum number K is approximately conserved, and eigenstates are expressed in the form of

K-mixing,

$$|i,IM\rangle = \sum_K g^{(i)}_{IK}|IMK\rangle. \tag{14}$$

The coefficients $g^{(i)}_{IK}$ are determined by solving the Hill-Wheeler equation

$$\sum_{K'}\left(H^I_{KK'} - E^i N^I_{KK'}\right)g^{(i)}_{IK'} = 0, \tag{15}$$

where the Hamiltonian and Norm elements are as follows:

$$H^I_{KK'} = \langle\psi|\hat{P}^n\hat{P}^z\hat{H}\hat{P}^I_{KK'}|\psi\rangle, \tag{16}$$

$$N^I_{KK'} = \langle\psi|\hat{P}^n\hat{P}^z\hat{P}^I_{KK'}|\psi\rangle. \tag{17}$$

Using Eqs. (12) and (13), we get the more detailed expressions

$$H^I_{KK'} = \frac{2I+1}{32\pi^4}\int d\Omega d\varphi_1 d\varphi_2 D^I_{MK}(\Omega) \times e^{-i(n_0\varphi_1+z_0\varphi_2)}\mathcal{H}(\Omega,\varphi_1,\varphi_2), \tag{18}$$

$$N^I_{KK'} = \frac{2I+1}{32\pi^4}\int d\Omega d\varphi_1 d\varphi_2 D^I_{MK}(\Omega) \times e^{-i(n_0\varphi_1+z_0\varphi_2)}\mathcal{N}(\Omega,\varphi_1,\varphi_2), \tag{19}$$

where

$$\mathcal{H}(\Omega,\varphi_1,\varphi_2) = \langle\psi|e^{i\varphi_1\hat{n}}e^{i\varphi_2\hat{z}}\hat{H}\hat{R}(\Omega)|\psi\rangle \tag{20}$$

and

$$\mathcal{N}(\Omega,\varphi_1,\varphi_2) = \langle\psi|e^{i\varphi_1\hat{n}}e^{i\varphi_2\hat{z}}\hat{R}(\Omega)|\psi\rangle \tag{21}$$

denote the energy and norm kernels, respectively.

In Eq. (10), the hypernuclear intrinsic wave function is divided into two parts: the BCS vacuum state $|\varphi\rangle_N$ for the core nucleus and the single-particle wave function $|\varphi\rangle_\Lambda$ for the Λ. Because the particle number is conserved for $|\varphi\rangle_\Lambda$, but not for $|\varphi\rangle_N$, the AMP and PNP operators both act on $|\varphi\rangle_N$ and just the AMP operator acts on $|\varphi\rangle_\Lambda$. Then the norm kernel in Eq. (21) is separated into two parts as

$$\mathcal{N}(\Omega,\varphi_1,\varphi_2) = \mathcal{N}_N\mathcal{N}_\Lambda \tag{22}$$

with

$$\mathcal{N}_N = \langle\varphi_N|e^{i\varphi_1\hat{n}}e^{i\varphi_2\hat{z}}\hat{R}(\Omega)|\varphi_N\rangle, \tag{23}$$

$$\mathcal{N}_\Lambda = \langle\varphi_\Lambda|\hat{R}(\Omega)|\varphi_\Lambda\rangle. \tag{24}$$

The algorithm to calculate the norm kernel $\mathcal{N}_N$ for the core nucleus is introduced in Refs. [43–46] in detail, while $\mathcal{N}_\Lambda$ is determined through the overlap of nonrotated, φ_Λ, and rotated, $\tilde{\varphi}_\Lambda$, hyperonic single-particle wave functions, which is analogous to Eq. (16) of Ref. [47]:

$$\mathcal{N}_\Lambda = \int d^3\boldsymbol{r}\sum_\sigma \varphi^*_\Lambda(\boldsymbol{r},\sigma)\tilde{\varphi}_\Lambda(\boldsymbol{r},\sigma). \tag{25}$$

Since the Hamiltonian is density dependent, in order to compute the energy kernel $\mathcal{H}$ it is necessary to transform the densities $\rho_\tau, \tau_\tau, \boldsymbol{J}_\tau, \boldsymbol{s}_\tau$ into transition densities, as is the case in Refs. [45,47]. The contribution from time-odd terms is taken into account in the energy kernel, although it vanishes in the mean-field calculation due to the time-reversal symmetry.

In our current calculation, we employ two simplifications of the procedure described so far. The first one is that the shape of the mean field is constrained to be axially symmetric. The second one is that we discard the K-mixing procedure, which is motivated by the fact that the single-particle wave function of the hyperon possesses an approximately good quantum number $K = 1/2$ and the intrinsic wave function of the nuclear core has a quantum number $K = 0$ due to the time-reversal symmetry assumed in the mean-field calculation.

Finally, through the projection, we can obtain the projected energy spectra

$$E_{I,1/2} = \frac{H^I_{1/2,1/2}}{N^I_{1/2,1/2}} \tag{26}$$

and $E2$ transition probabilities

$$B(E2, I_i \to I_f) = \frac{1}{2I_i+1}|\langle f; I_f||\hat{Q}_2||i; I_i\rangle|^2, \tag{27}$$

where

$$\langle f; I_f||\hat{Q}_2||i; I_i\rangle = \sqrt{2I_f+1}\sum_{M\mu} C^{I_fK_f}_{I_iM2\mu}\langle\psi|P^{\hat{n}}P^{\hat{z}}\hat{O}_{2\mu}\hat{P}^{I_i}_{MK_i}|\psi\rangle, \tag{28}$$

in which $\hat{O}_{2\mu} = r^2Y_{2\mu}(\varphi,\theta)$ is the electric quadrupole transition operator [47] and $C^{I_fK_f}_{I_iM2\mu}$ denotes the Clebsch-Gordon coefficients.

In our current work, the deformation parameter β is calculated using the first-order approximation [47] and extracted from the mean-field calculation. Assuming a nucleus an axial rigid rotor, the reduced $E2$ transition probability from a $(I+2)^+$ state to a I^+ state is expressed as [26,35,47]

$$B(E2) = \frac{15}{32\pi}\frac{(I+1)(I+2)}{(2I+3)(2I+5)}Q^2_p, \tag{29}$$

where

$$Q_p = \sqrt{\frac{5}{\pi}}Z\beta R^2_p \tag{30}$$

is the electric quadrupole moment, with Z the proton number, R_p the root-mean-square charge radius, and β the quadrupole deformation parameter of the electric charge distribution of the nucleus. One thus finds that $B(E2)$ is proportional to R^4_p and β^2.

In our current calculations, we choose the parameters as follows. We use the SGII Skyrme force, which was introduced to reproduce the nuclear compression modulus [48] for the NN interaction and the NSC89 force for the $N\Lambda$ interaction. Other Skyrme forces (SLy4 and SIII) were also tested and similar results were obtained for ${}^{13}_{\Lambda}$C and ${}^{25}_{\Lambda}$Mg using the mean-field calculation, but are not shown in this paper for brevity. For ^{12}C, ${}^{13}_{\Lambda}$C, ^{20}Ne, and ${}^{21}_{\Lambda}$Ne, the strength of the pairing force is $V_0 = -410$ MeV for both neutrons and protons and the strength of the spin-orbit term in the SGII force is reduced by a factor of 0.6 for ^{12}C and ${}^{13}_{\Lambda}$C to reproduce their oblate shapes as in Refs. [26,49,50]. For heavier (hyper)nuclei the strength of the pairing force is chosen as $V_0 = -1000$ MeV [32]. For

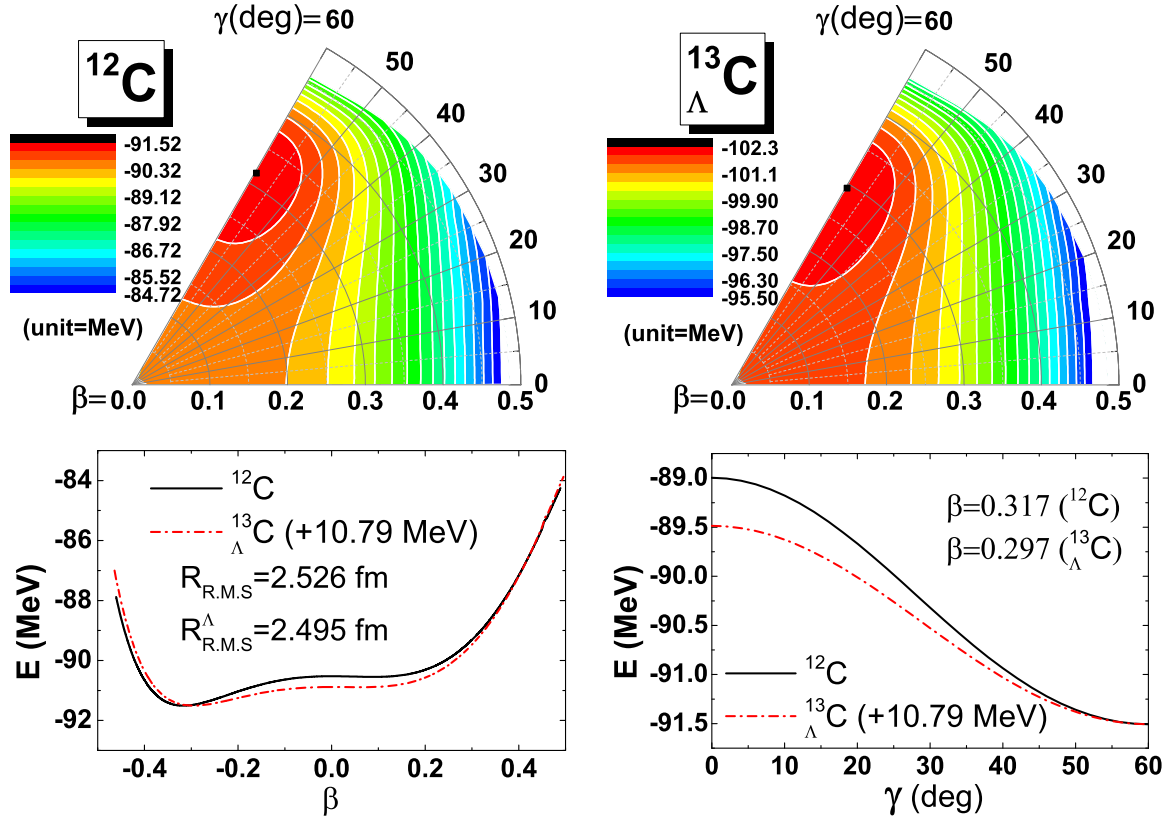

FIG. 1. (Color online) (Top row) The PES pattern in the (β,γ) plane for ^{12}C (left) and $^{13}_{\Lambda}$C (right). Contour lines are separated by 0.4 MeV. (Bottom row) Binding energy in the β direction (left) and γ direction (right; β is fixed at the energy minimum point [black dot]). Nuclear root-mean-square radii are given for core nucleus ($R_{\rm RMS}$) and core of the hypernucleus ($R^{\Lambda}_{\rm RMS}$).

all calculations a smooth pairing energy cutoff of 5.0 MeV around the Fermi surface is used [32,51].

III. RESULTS

A. Mean-field calculation

Solving the shape-constrained mean-field equation (4), one obtains the PES of each (hyper)nucleus with respect to certain quadrupole shapes. In order to show the effects caused by the addition of a Λ to a nuclear system, Fig. 1 compares the PES of ^{12}C and $^{13}_{\Lambda}$C in the (β,γ) plane and in the directions of β and γ. One can see that the shapes of ^{12}C and $^{13}_{\Lambda}$C are both oblate with β being -0.317 and -0.297, respectively, and the energy change due to the hyperon is about 10.8 MeV, which corresponds to the experimental value [52]. Compared with ^{12}C the PES of $^{13}_{\Lambda}$C in γ direction becomes flatter. These phenomena are nearly identical to those obtained in Ref. [32].

The added hyperon in a nearly spherical $s_{1/2}$ state thus causes two effects: it slightly reduces both the quadrupole deformation β and the nuclear core radius $R_{\rm RMS}$. The root-mean-square radii and β values are listed in Table I for the various (hyper)nuclei we are considering in this article.

Figure 2 shows the deformation properties of ^{20}Ne and $^{21}_{\Lambda}$Ne. Compared to ^{12}C, the deformation is prolate and the added Λ causes smaller changes of $R_{\rm RMS}$ and β, because the energy minimum of ^{20}Ne is deeper than that of ^{12}C, which indicates a more stable ground state.

A similar behavior is predicted for ^{24}Mg and $^{25}_{\Lambda}$Mg in Fig. 3, which have also been investigated by both the AMD method [14–16] and the SHF+BCS model of Ref. [32]. Compared with the results given in the latter reference, the NSC89 $N\Lambda$ interaction chosen in this paper is weaker than the Skyrme-type $N\Lambda$ interaction to polarize the core nucleus.

In contrast, ^{28}Si and $^{29}_{\Lambda}$Si, displayed in Fig. 4, are both oblate and opposite compared to ^{24}Mg and $^{25}_{\Lambda}$Mg, which can be understood by the different characteristics of the splitting of the last occupied $d_{5/2}$ orbit in the oblate and prolate regions, as shown in Fig. 5: In the prolate region, 3/2[211] and 1/2[220] decrease while 5/2[202] increases, but in the oblate region, those three orbits do not split much and change slowly when

TABLE I. Root-mean-square radii $R_{\rm RMS}$ and deformation β of the nuclear core in various (hyper)nuclei.

	^{12}C	$^{13}_{\Lambda}$C	Ratio	^{20}Ne	$^{21}_{\Lambda}$Ne	Ratio	^{24}Mg	$^{25}_{\Lambda}$Mg	Ratio	^{26}Mg	$^{27}_{\Lambda}$Mg	Ratio	^{26}Si	$^{27}_{\Lambda}$Si	Ratio	^{28}Si	$^{29}_{\Lambda}$Si	Ratio
$R_{\rm RMS}$	2.526	2.495	0.952	2.861	2.845	0.978	2.980	2.969	0.986	2.976	2.963	0.983	2.989	2.976	0.982	3.051	3.038	0.983
β	−0.317	−0.297	0.878	0.396	0.388	0.960	0.409	0.401	0.961	−0.229	−0.219	0.915	−0.233	−0.223	0.916	−0.283	−0.274	0.937

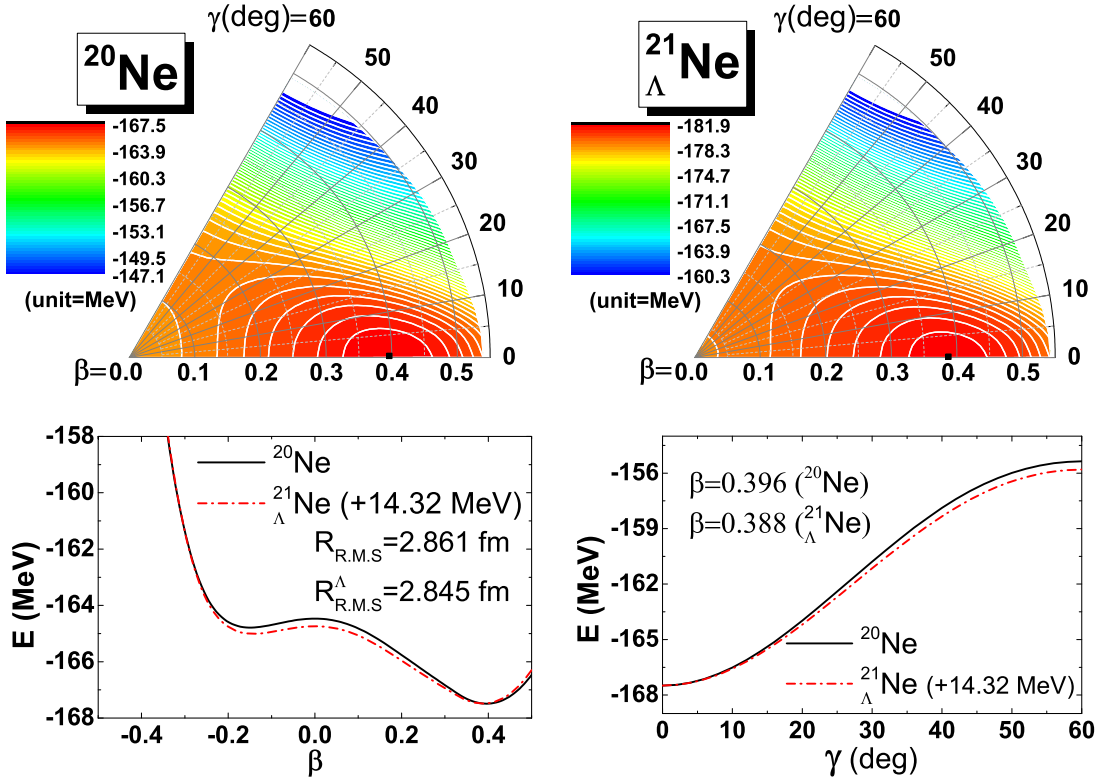

FIG. 2. (Color online) As Fig. 1, but for ^{20}Ne and $^{21}_{\Lambda}$Ne.

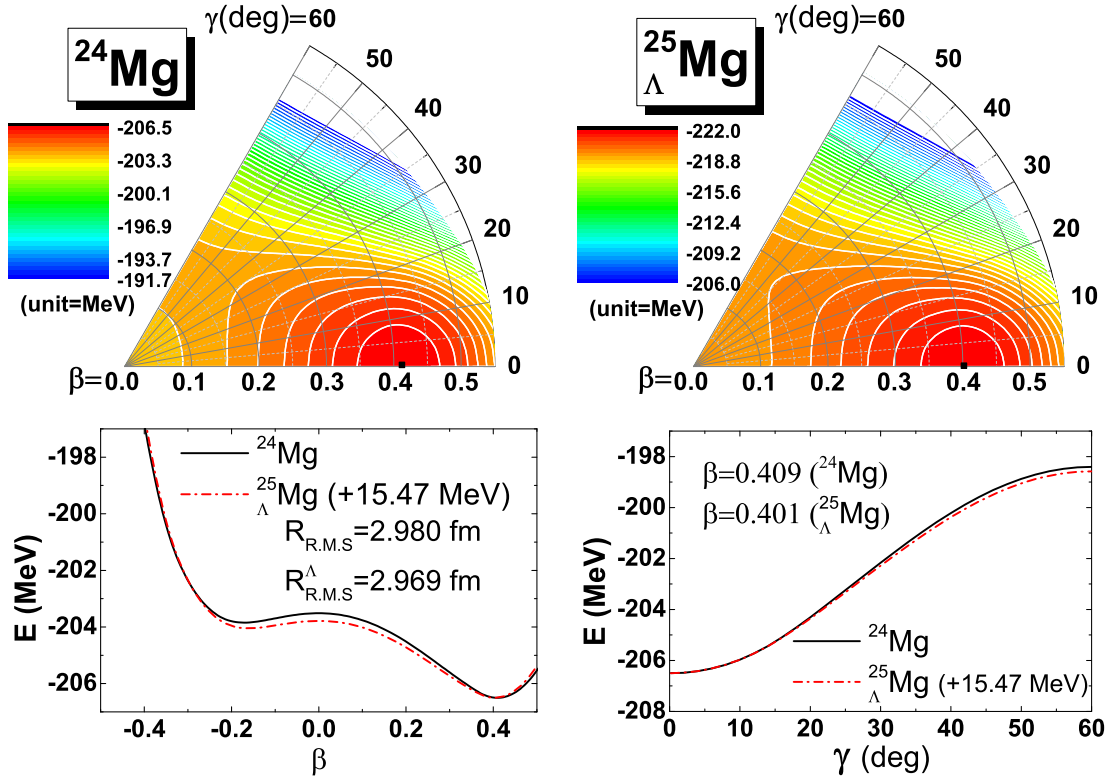

FIG. 3. (Color online) As Fig. 1, but for ^{24}Mg and $^{25}_{\Lambda}$Mg.

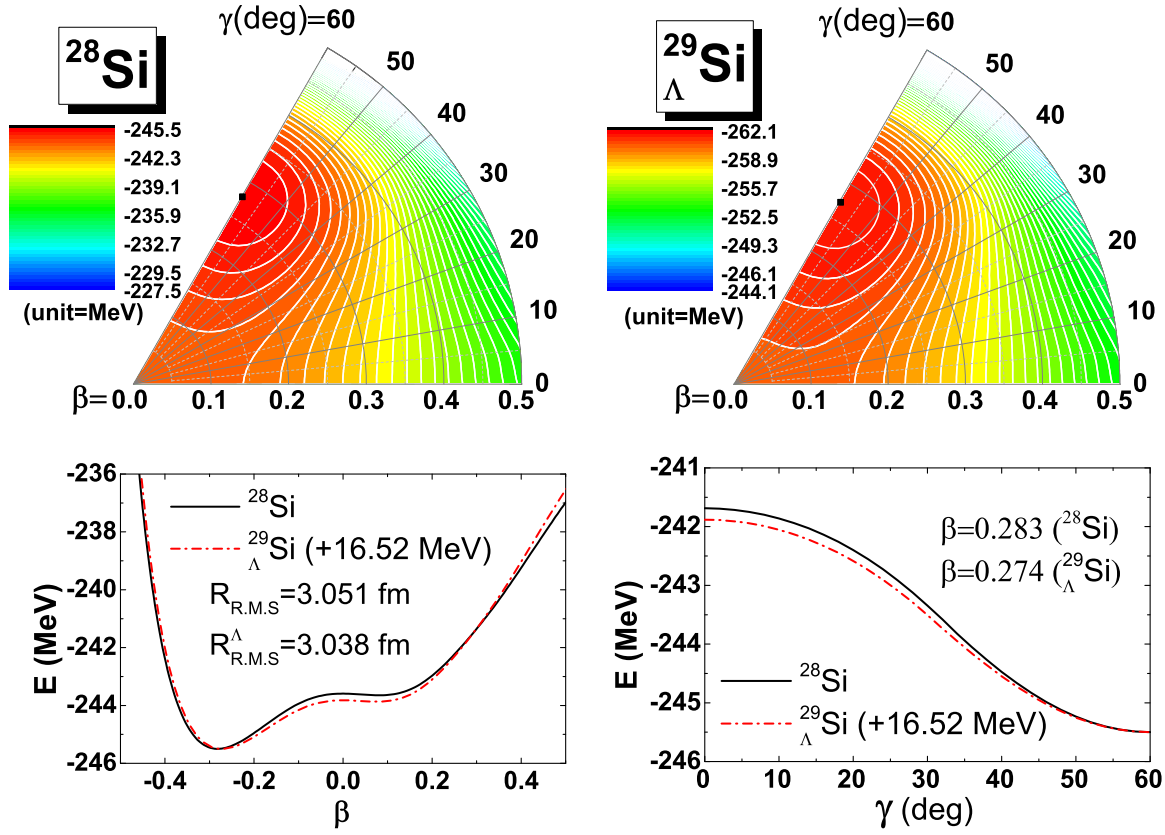

FIG. 4. (Color online) As Fig. 1, but for ^{28}Si and $^{29}_{\Lambda}$Si.

β changes from -0.2 to -0.3. Thus if the particle numbers of protons and neutrons are 12, the two fast decreasing orbits on the prolate side are occupied, and if they are 14, the three orbits in the oblate region will be occupied to obtain a lower energy. That is why ^{24}Mg and ^{28}Si have different shapes.

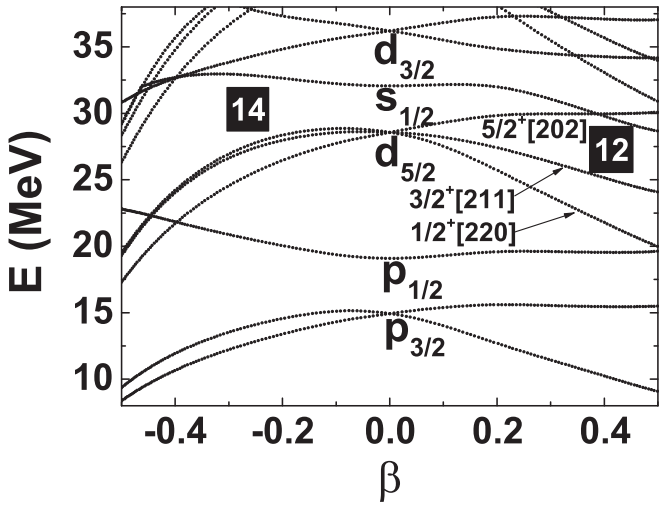

FIG. 5. Single-particle neutron levels versus quadrupole deformation β for ^{28}Si, relative to the energy of the $1s_{1/2}$ level. The proton levels and also the levels of ^{24}Mg have similar trends as in this figure. The labels "12" and "14" denote the positions of the energy minima of ^{24}Mg and ^{28}Si, respectively.

Due to this competition between prolate and oblate shapes, the mirror nuclei ^{26}Mg and ^{26}Si, shown in Figs. 6 and 7, both have a γ-soft shape, and the addition of a Λ makes the corresponding hypernuclei even softer in the γ direction. Although the addition of one Λ does not change the prolate minima of these two nuclei in our calculation or in the results given in Ref. [32], the shapes of such kinds of γ-soft nuclei will be much easier to change than those of nuclei stable in their shape minima.

B. Energy spectra

In the last subsection, we have discussed the results of the SHF+BCS model, but the solution of such a mean-field model loses the angular momentum quantum number and breaks the particle number conservation, which makes it unrealistic to investigate hypernuclear energy spectra and transition probabilities. As introduced in Sec. II, AMP and PNP methods can restore these symmetries, and in this subsection we use these projection techniques to obtain the energy spectra and $E2$ transition probabilities of hypernuclei. In our current calculation the GCM and K mixing are not included, so we just obtain the ground bands ($[J^{+}_{\text{g.s.}} \otimes s_{\Lambda}]$) of hypernuclei.

Table II lists the energy spectra of ^{12}C, $^{13}_{\Lambda}$C, ^{20}Ne, $^{21}_{\Lambda}$Ne, ^{24}Mg, $^{25}_{\Lambda}$Mg, ^{28}Si, and $^{29}_{\Lambda}$Si. Due to the degeneracy of spin doublets of a hypernucleus, which is caused by the exclusion of hyperonic spin-orbit terms, the spin doublets are denoted by the spin of the core nucleus for convenience. The observed and calculated results are labeled by "exp" and "cal", respectively.

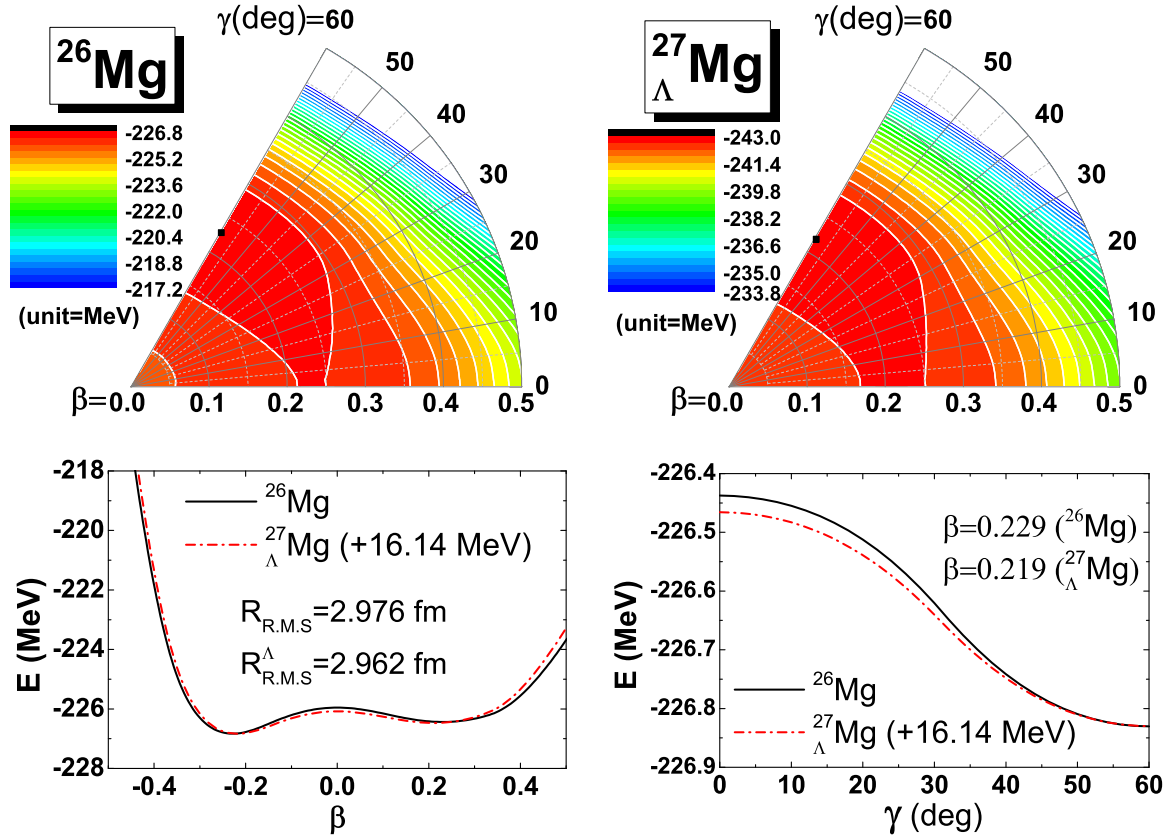

FIG. 6. (Color online) As Fig. 1, but for ^{26}Mg and $^{27}_{\Lambda}$Mg.

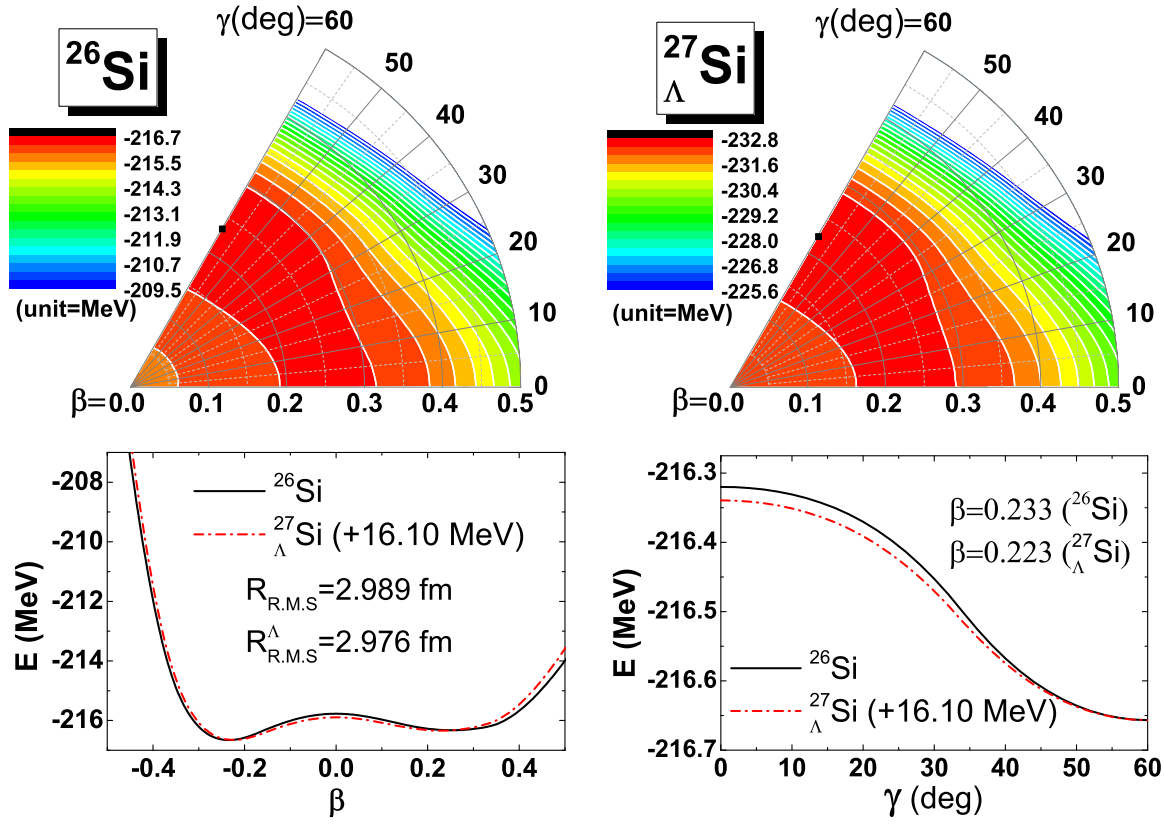

FIG. 7. (Color online) As Fig. 1, but for ^{26}Si and $^{27}_{\Lambda}$Si.

TABLE II. Observed (exp) [53] and calculated (cal) energy levels (in MeV) for different (hyper)nuclei.

	^{12}C		$^{13}_{\Lambda}$C	^{20}Ne		$^{21}_{\Lambda}$Ne	^{24}Mg		$^{25}_{\Lambda}$Mg	^{28}Si		$^{29}_{\Lambda}$Si
I^+	exp	cal	cal	exp	cal	cal	exp	cal	cal	exp	cal	cal
2^+	4.44	3.16	3.25	1.63	1.01	0.99	1.37	1.15	1.13	1.78	1.70	1.77
4^+	14.08	10.02	10.05	4.25	3.48	3.40	4.12	3.97	3.92	4.62	5.45	5.64
6^+				8.78	7.97	7.80	8.11	8.75	8.69	8.54	11.06	11.37

One observes that in most cases the calculated energies are smaller than the observed ones. This compression of the calculated energy spectrum is mainly due to the collapse of the pairing correlations for the projected configuration. This is proven by the stretched energy spectrum of ^{24}Mg in Ref. [45], where the pairing collapse is prevented by the Lipkin-Nogami method. On the other hand, the introduction of the GCM can also stretch the energy spectrum to some extent, especially for β-soft nuclei, which is demonstrated by the calculated energy spectra of ^{24}Mg in Refs. [45,46], where the energies of the 2^+ state were indeed shifted by the GCM. As discussed above, the GCM is important for β-soft nuclei, and the PES pattern in the last subsection demonstrated that the shape of ^{12}C is softer than those of ^{20}Ne, ^{24}Mg, and ^{28}Si. That explains why the discrepancy between observed and calculated values is more pronounced for this nucleus. Table II also shows that the addition of one Λ causes only small changes of tens of KeV to the energy levels.

Using the projected wave functions and Eq. (27), we list in Table III the $E2$ transition probabilities within the ground bands of ^{12}C, ^{20}Ne, ^{24}Mg, ^{28}Si, and of their corresponding hypernuclei. The observed deviations from the experimental values may be eliminated in part when the GCM method is used. Due to the splitting of angular momentum $J = J'$ into $J = J' \pm 1/2$, each of the $B(E2)$ values of the core nucleus has two counterparts in hypernuclei, and they are both listed.

The addition of one Λ thus reduces slightly the $B(E2)$ values and this shrinkage effect is characterized by the value of Γ_B [14,54], defined as

$$\Gamma_B = \frac{B(E2, I_{ic}^+ \to I_{fc}^+)_H}{B(E2, I_i^+ \to I_f^+)}, \tag{31}$$

where $B(E2, I_i^+ \to I_f^+)$ and $B(E2, I_{ic}^+ \to I_{fc}^+)_H$ represent reduced $E2$ transition probabilities of the ordinary nucleus and the nuclear core in the hypernucleus, respectively. The table shows the Γ_B values of each nucleus and all are smaller than 1. For example, the Γ_B value of the core nucleus in $^{25}_{\Lambda}$Mg is 0.925, which indicates that the Λ hyperon decreases the $E2$ transition strength from the 2_1^+ state to the ground state by 7.5%, compared to a reduction of 17% obtained in the previous work based on the relativistic EDF [21], demonstrating a stronger impurity effect of the Λ hyperon in the RMF.

According to Eqs. (29) and (30), the $B(E2)$ value is proportional to $R_{\rm RMS}^4$ and to β^2, therefore both the shrinkage of the nuclear size, indicated by $R_{\rm RMS}$, and the reduction of the quadrupole deformation β are responsible for the overall reduction of $B(E2)$. To see which effect is dominant, we list in Table IV also the "Ratios" $(R_{\rm RMS}^{\Lambda}/R_{\rm RMS}^{\rm no\,\Lambda})^4$ and $(\beta^{\Lambda}/\beta^{\rm no\,\Lambda})^2$, as extracted from the mean-field calculation. One finds that in fact the reduction of β is more important than that of $R_{\rm RMS}$ for all nuclei considered.

The calculation in this paper also shows that the shrinkage effect diminishes with the mass number of the nucleus, since the attraction of a single Λ embedded in the center has only limited range and hardly affects a heavy nucleus. In fact Ref. [54] showed a much stronger reduction effect, $\Gamma_B \approx 0.32$, for the very light $^{7}_{\Lambda}$Li hypernucleus.

IV. CONCLUSION AND OUTLOOK

We combined the triaxially shape-constrained SHF+BCS mean-field model and the density-dependent NSC89 $N\Lambda$ interaction to investigate the PES of various hypernuclei. We found that, in general, the addition of one Λ reduces slightly the quadrupole shape of a nuclear system. From $^{13}_{\Lambda}$C to $^{29}_{\Lambda}$Si the change of β due to the addition of a Λ decreases, because the stability of the respective core nuclei increases. The PES of ^{26}Mg and ^{26}Si have γ-soft patterns due to the competition between oblate and prolate energy minima, and the addition of a Λ does not change such patterns significantly.

The AMP and PNP techniques were used in this paper to restore the rotational symmetry and particle number conservation broken in the SHF calculation and BCS approximation, respectively. This made it possible to study the hypernuclear energy spectra in the laboratory-fixed reference frame. The

TABLE III. Experimental (exp) [53] and calculated (cal) $B(E2)$ values (in units of W.u.) for different (hyper)nuclei. The ratios Γ_B defined by Eq. (31) are also given to show the shrinkage effect.

		^{12}C		$^{13}_{\Lambda}$C		^{20}Ne		$^{21}_{\Lambda}$Ne		^{24}Mg		$^{25}_{\Lambda}$Mg		^{28}Si		$^{29}_{\Lambda}$Si	
$I_i^P \to I_f^P$		exp	cal	cal	Γ_B	exp	cal	cal	Γ_B	exp	cal	cal	Γ_B	exp	cal	cal	Γ_B
$2^+ \to 0^+$	$\frac{3^+/2 \to 1^+/2}{5^+/2 \to 1^+/2}$	4.65(26)	6.42	$\frac{5.61}{5.69}$	0.885	20.3(10)	18.89	$\frac{17.72}{17.72}$	0.932	21.5(10)	24.30	$\frac{22.50}{22.72}$	0.925	13.2(5)	14.23	$\frac{13.27}{13.27}$	0.929
$4^+ \to 2^+$	$\frac{7^+/2 \to 3^+/2}{9^+/2 \to 5^+/2}$		10.11	$\frac{8.23}{8.84}$	0.898	22.0(2)	27.69	$\frac{23.09}{25.73}$	0.938	39.0(4)	35.45	$\frac{29.83}{33.05}$	0.937	16.4(18)	21.46	$\frac{18.09}{20.23}$	0.930
$6^+ \to 4^+$	$\frac{11^+/2 \to 7^+/2}{13^+/2 \to 9^+/2}$					20.0(3)	31.78	$\frac{28.45}{29.46}$	0.929		41.15	$\frac{36.82}{38.34}$	0.945	10.6(10)	25.75	$\frac{23.29}{24.44}$	0.948

TABLE IV. Root-mean-square radius $R_{\rm RMS}$ and quadrupole parameter β of the charge distributions in various (hyper)nuclei. The "Ratio" corresponding to the change of radii is defined as $(R^{\Lambda}_{\rm RMS}/R^{\rm no\,\Lambda}_{\rm RMS})^4$, and the one corresponding to β as $(\beta^{\Lambda}/\beta^{\rm no\,\Lambda})^2$.

	^{12}C	$^{13}_{\Lambda}$C	Ratio	^{20}Ne	$^{20}_{\Lambda}$Ne	Ratio	^{24}Mg	$^{25}_{\Lambda}$Mg	Ratio	^{28}Si	$^{29}_{\Lambda}$Si	Ratio
$R_{\rm RMS}$	2.604	2.565	0.941	2.939	2.918	0.972	3.051	3.032	0.975	2.976	2.963	0.981
β	−0.385	−0.367	0.909	0.484	0.473	0.953	0.481	0.470	0.952	−0.333	−0.325	0.952

related $E2$ transition probabilities were found to be slightly reduced by adding a Λ, due to the corresponding reduction of both the charge radius $R_{\rm RMS}$ and the quadrupole deformation β. The latter change was shown to be the dominant one for all nuclei considered.

In the future, we plan to extend the projecting calculation to triaxial nuclear shape and also to take the K mixing into consideration, in order to determine more precisely the energy minima of some potentially triaxially deformed nuclei, for example ^{24}Mg. Furthermore, the theoretical results obtained in Sec. III predict a 2^+ state of ^{12}C that is lower than the observed one, which we attribute to the absence of coupling of states with different quadrupole shapes. This could be improved by the introduction of the GCM, which is also required for the energy spectrum investigation of some γ-soft hypernuclei, such as $^{27}_{\Lambda}$Mg and $^{27}_{\Lambda}$Si. Finally, hyperonic excited states such as $[^{12}C_{\rm g.s.}(0^+) \otimes p_{\Lambda}]$ could be investigated by taking the p_{Λ} single-particle wave function into consideration.

ACKNOWLEDGMENTS

The authors thank E. Hiyama and S.-G. Zhou for helpful discussions. This work was supported by the National Natural Science Foundation of China (Grants No. 10975116 and No. 11275160) and Open Project Program of State Key Laboratory of Theoretical Physics, Institute of Theoretical Physics, Chinese Academy of Sciences, China (No. Y5KF141CJ1). Partial support comes from "NewCompStar," COST Action MP1304.

[1] O. Hashimoto and H. Tamura, Prog. Part. Nucl. Phys. **57**, 564 (2006).
[2] H. Kohri *et al.*, Phys. Rev. C **65**, 034607 (2002).
[3] K. Tanida *et al.*, Phys. Rev. Lett. **86**, 1982 (2001).
[4] A. Gal, J. M. Soper, and R. H. Dalitz, Ann. Phys. (NY) **63**, 53 (1971); **72**, 445 (1972); **113**, 79 (1978).
[5] R. H. Dalitz and A. Gal, Ann. Phys. (NY) **116**, 167 (1978).
[6] D. J. Millener, A. Gal, C. B. Dover, and R. H. Dalitz, Phys. Rev. C **31**, 499 (1985).
[7] V. N. Fetisov, L. Majling, J. Žofka, and R. A. Eramzhyan, Z. Phys. A **339**, 399 (1991).
[8] D. J. Millener, Nucl. Phys. A **804**, 84 (2008).
[9] E. Hiyama, M. Kamimura, T. Motoba, T. Yamada, and Y. Yamamoto, Phys. Rev. C **66**, 024007 (2002).
[10] Y. Kanada-En'yo, H. Horiuchi, and A. Ono, Phys. Rev. C **52**, 628 (1995).
[11] E. Hiyama, M. Kamimura, T. Motoba, T. Yamada, and Y. Yamamoto, Phys. Rev. Lett. **85**, 270 (2000).
[12] E. Hiyama, Y. Yamamoto, T. Motoba, and M. Kamimura, Phys. Rev. C. **80**, 054321 (2009).
[13] E. Hiyama, M. Kamimura, Y. Yamamoto, and T. Motoba, Phys. Rev. Lett. **104**, 212502 (2010).
[14] M. Isaka, M. Kimura, A. Doté, and A. Ohnishi, Phys. Rev. C **83**, 044323 (2011); **83**, 054304 (2011).
[15] M. Isaka, H. Homma, M. Kimura, A. Dote, and A. Ohnishi, Phys. Rev. C **85**, 034303 (2012).
[16] M. Isaka, M. Kimura, A. Dote, and A. Ohnishi, Phys. Rev. C **87**, 021304(R) (2013).
[17] M.-T. Win and K. Hagino, Phys. Rev. C **78**, 054311 (2008).
[18] B.-N. Lu, E.-G. Zhao, and S.-G. Zhou, Phys. Rev. C **84**, 014328 (2011).
[19] B.-N. Lu, E. Hiyama, H. Sagawa, and S.-G. Zhou, Phys. Rev. C **89**, 044307 (2014).
[20] H. Mei, K. Hagino, J. M. Yao, and T. Motoba, Phys. Rev. C **90**, 064302 (2014).
[21] W. X. Xue, J. M. Yao, K. Hagino, Z. P. Li, H. Mei, and Y. Tanimura, Phys. Rev. C **91**, 024327 (2015).
[22] J. Cugnon, A. Lejeune, and H.-J. Schulze, Phys. Rev. C **62**, 064308 (2000).
[23] I. Vidaña, A. Polls, A. Ramos, and H.-J. Schulze, Phys. Rev. C **64**, 044301 (2001).
[24] X.-R. Zhou, H.-J. Schulze, H. Sagawa, C.-X. Wu, and E.-G. Zhao, Phys. Rev. C **76**, 034312 (2007).
[25] X.-R. Zhou, A. Polls, H.-J. Schulze, and I. Vidana, Phys. Rev. C **78**, 054306 (2008).
[26] H.-J. Schulze, M. Thi Win, K. Hagino, and H. Sagawa, Prog. Theor. Phys. **123**, 569 (2010).
[27] H.-J. Schulze, Nucl. Phys. A **835**, 19 (2010).
[28] H.-J. Schulze and T. Rijken, Phys. Rev. C **88**, 024322 (2013).
[29] H.-J. Schulze, M. Baldo, U. Lombardo, J. Cugnon, and A. Lejeune, Phys. Rev. C **57**, 704 (1998).
[30] H.-J. Schulze and T. Rijken, Phys. Rev. C **84**, 035801 (2011).
[31] M. Rayet, Nucl. Phys. A **367**, 381 (1981).
[32] M.-T. Win, K. Hagino, and T. Koike, Phys. Rev. C **83**, 014301 (2011).
[33] J. M. Yao, Z. P. Li, K. Hagino, M.-T. Win, Y. Zhang, and J. Meng, Nucl. Phys. A **868-869**, 12 (2011).
[34] W. Greiner and J. A. Maruhn, *Nuclear Models* (Springer, Berlin, 1996), p. 281.
[35] P. Ring and P. Schuck, *The Nuclear Many-Body Problem* (Springer, Berlin, 1980)
[36] J. Dobaczewski and J. Dudek, Comput. Phys. Commun. **102**, 166 (1997); **102**, 183 (1997).
[37] P. Bonche, H. Flocard, and P. H. Heenen, Nucl. Phys. A **467**, 115 (1987).
[38] T. Motoba, D. E. Lanskoy, D. J. Millener, and Y. Yamamoto, Nucl. Phys. A **804**, 99 (2008).

[39] F. Cusanno *et al.*, Phys. Rev. Lett. **103**, 202501 (2009).
[40] N. Tajima, P. Bonche, H. Flocard, P.-H. Heenen, and M. S. Weiss, Nucl. Phys. A **551**, 434 (1993).
[41] M. Bender, K. Rutz, P.-G. Reinhard, and J. A. Maruhn, Eur. Phys. J. A **8**, 59 (2000).
[42] K. Hara and Y. Sun, Int. J. Mod. Phys. E **04**, 637 (1995).
[43] P. Bonche, J. Dobaczewski, H. Flocard, P.-H. Heenen, and J. Meyer, Nucl. Phys. A **510**, 466 (1990).
[44] P.-H. Heenen, P. Bonche, J. Dobaczewski, and H. Flocard, Nucl. Phys. A **561**, 367 (1993).
[45] A. Valor, P.-H. Heenen, and P. Bonche, Nucl. Phys. A **671**, 145 (2000).
[46] M. Bender and P.-H. Heenen, Phys. Rev. C **78**, 024309 (2008).
[47] J. Dobaczewski *et al.*, Comput. Phys. Commun. **180**, 2361 (2009).
[48] N. Van Giai and H. Sagawa, Phys. Lett. B **106**, 379 (1981).
[49] H. Sagawa, X.-R. Zhou, X.-Z. Zhang, and T. Suzuki, Phys. Rev. C **70**, 054316 (2004).
[50] Y. Zhang, H. Sagawa, D. Yoshino, K. Hagino, and J. Meng, Prog. Theor. Phys. **120**, 129 (2008).
[51] J. Terasaki, P.-H. Heenen, H. Flocard, and P. Bonche, Nucl. Phys. A **600**, 371 (1996).
[52] M. Agnello *et al.*, Phys. Lett. B **698**, 219 (2011).
[53] National Nuclear Data Center, http://www.nndc.bnl.gov/
[54] E. Hiyama, M. Kamimura, K. Miyazaki, and T. Motoba, Phys. Rev. C **59**, 2351 (1999).